

Fully automatic spatiotemporal segmentation of 3D LiDAR time series for the extraction of natural surface changes

Anders, Katharina; Winiwarter, Lukas; Mara, Hubert; Lindenbergh, Roderik; Vos, Sander E.; Höfle, Bernhard

DOI

[10.1016/j.isprsjprs.2021.01.015](https://doi.org/10.1016/j.isprsjprs.2021.01.015)

Publication date

2021

Document Version

Final published version

Published in

ISPRS Journal of Photogrammetry and Remote Sensing

Citation (APA)

Anders, K., Winiwarter, L., Mara, H., Lindenbergh, R., Vos, S. E., & Höfle, B. (2021). Fully automatic spatiotemporal segmentation of 3D LiDAR time series for the extraction of natural surface changes. *ISPRS Journal of Photogrammetry and Remote Sensing*, 173, 297-308.
<https://doi.org/10.1016/j.isprsjprs.2021.01.015>

Important note

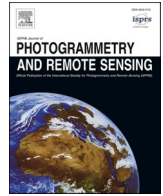
To cite this publication, please use the final published version (if applicable).
Please check the document version above.

Copyright

Other than for strictly personal use, it is not permitted to download, forward or distribute the text or part of it, without the consent of the author(s) and/or copyright holder(s), unless the work is under an open content license such as Creative Commons.

Takedown policy

Please contact us and provide details if you believe this document breaches copyrights.
We will remove access to the work immediately and investigate your claim.



Fully automatic spatiotemporal segmentation of 3D LiDAR time series for the extraction of natural surface changes

Katharina Anders^{a,b,*}, Lukas Winiwarter^a, Hubert Mara^{b,c}, Roderik Lindenbergh^d, Sander E. Vos^e, Bernhard Höfle^{a,b,f}

^a 3D Geospatial Data Processing Group (3DGeo), Institute of Geography, Heidelberg University, Germany

^b Interdisciplinary Center for Scientific Computing (IWR), Heidelberg University, Germany

^c i3mainz – Institute for Spatial Information and Surveying Technology, Mainz University Of Applied Sciences, Germany

^d Department of Geoscience & Remote Sensing, Delft University of Technology, the Netherlands

^e Department of Hydraulic Engineering, Delft University of Technology, the Netherlands

^f Heidelberg Center for the Environment (HCE), Heidelberg University, Germany

ARTICLE INFO

Keywords:

4D object-by-change
Point clouds
Terrestrial laser scanning
Change detection
Coastal monitoring

ABSTRACT

Geographic observation benefits from the increasing availability of time series of 3D geospatial data, which allow analysis of change processes at high temporal detail and over extensive periods. In this context, the demand for advanced methods to detect and extract topographic surface changes from these 4D geospatial data emerges. Changes in natural scenes occur with varying magnitude, duration, spatial extent, and change rate, and the timing of their occurrence is not known. Standard pairwise change detection requires the selection of fixed analysis periods and the specification of magnitude thresholds to determine accumulation or erosion forms. In settings with continuous surface morphology and dynamic changes to the surface due to material transport, such change forms are typically temporary and may be missed or aggregated if they occur with spatial and/or temporal overlap. This is overcome with the extraction of 4D objects-by-change (4D-OBCs). These objects are obtained by firstly detecting surface changes in the temporal domain at locations in the scene. Subsequently, they are spatially delineated by considering the full history of surface change during region growing from the seed location of a detected change. To perform this spatiotemporal segmentation systematically for entire 3D time series, we develop a fully automatic approach of seed detection and selection, combined with locally adaptive thresholding for region growing of individual objects with varying change properties. We apply our workflow to a five-months hourly time series of around 3,000 terrestrial laser scanning point clouds acquired for coastal monitoring at a sandy beach in The Netherlands. This provides 2,021 4D-OBCs as extracted accumulation or erosion forms. Results are validated through majority agreement of six expert analysts, who evaluate the segmentation performance at sample locations throughout the scene. Accordingly, our method extracts surface changes with an error of omission of 4.7% and an error of commission of 16.6%. We examine the results and provide considerations how postprocessing of segments can further improve the change analysis workflow. The developed approach thereby provides a powerful tool for automatic change analysis in 4D geospatial data, namely to detect and delineate natural surface changes across space and time.

1. Introduction

Time series of topographic 3D data pose great possibilities to geographic analyses, but also challenges to the detection and delineation of surface change information from these 4D geospatial data. Surface change analysis using topographic point clouds has long since gained considerable importance in the observation of Earth surface processes

and in advancing geoscientific research in general (Eitel et al., 2016; Qin et al., 2016). Ongoing repetitions of topographic surveys have led to the cumulation of data in the temporal dimension that enable change detection for many use cases of Earth surface observation, among them studies of changes to landslides (Oppikofer et al., 2009; Pfeiffer et al., 2018), rockfalls (Abellán et al., 2010; Rosser et al., 2007), rock glaciers (Bodin et al., 2018; Zahs et al., 2019), snow cover (Grünwald et al.,

* Corresponding author at: 3DGeo at the Institute of Geography, Im Neuenheimer Feld 368, 69120 Heidelberg, Germany.

E-mail address: katharina.anders@uni-heidelberg.de (K. Anders).

<https://doi.org/10.1016/j.isprsjprs.2021.01.015>

Received 11 November 2020; Received in revised form 15 January 2021; Accepted 18 January 2021

Available online 8 February 2021

0924-2716/© 2021 International Society for Photogrammetry and Remote Sensing, Inc. (ISPRS). Published by Elsevier B.V. All rights reserved.

2010; Fey et al., 2019), and the coast (Fabbri et al., 2017; Miles et al., 2019).

Most recently, the acquisition strategy of permanent terrestrial laser scanning (TLS) generates time series of 3D point clouds at (sub-)hourly intervals over periods of weeks to months (e.g., Kromer et al., 2017; O’Dea et al., 2019; Stumvoll et al., 2020; Vos et al., 2017; Williams et al., 2018). Such high-frequency time series of point clouds can alternatively be acquired by photogrammetric techniques (e.g., Eltner et al., 2017; Kromer et al., 2019), albeit obtained datasets have different properties from laser scanning point clouds and may require other specific processing strategies. The unprecedented temporal density of these 4D datasets provides many more epochs for change analysis to compare evermore combinations of pairwise states of the topography, which are ideally adapted to the rates of target changes, respectively. Even more importantly, the information these data potentially contain on temporal properties of change processes hold opportunity for new insights on spatiotemporal characteristics of topographic activity and, consequently, to extend our fundamental knowledge about the investigated geographic phenomena (Eitel et al., 2016; Eltner et al., 2017).

To leverage the temporal dimension of 3D time series for change detection and delineation, a method of spatiotemporal segmentation was developed that makes use of the full history of surface change to extract periods and spatial extents of surface changes (Anders et al., 2020b). The time series-based approach is designed to advance established approaches of pairwise change detection. Pairwise change analysis typically serves to identify areas of accumulation or erosion over the selected analysis period and to quantify change rates. Based on the bitemporal change information, patterns and underlying drivers of change are interpreted (e.g., Anders et al., 2020a; Eltner et al., 2017; Fey et al., 2019; Zahr et al., 2019). Standard methods for pairwise change detection are the differencing of Digital Elevation Models (DEMs, James et al., 2012) or point cloud distance computation (Girardeau-Montaut et al., 2005; Lague et al., 2013). Alternatively, change can be assessed in object-based approaches, where observed objects are first identified based on morphometric features or even previously derived bitemporal surface change, and subsequently changes in object properties are analysed, such as their location and size (e.g., Mayr et al., 2018).

In the following, we reveal drawbacks of pairwise change detection methods for the analysis of 3D time series. These drawbacks arise from the general circumstance of observing natural, Earth shaping processes that it is not a priori known when and where changes occur within a scene, and what the spatial and temporal properties of these changes

are. The required selection of epochs in pairwise change analysis entails that the periods for detecting change are pre-defined. Temporary surface changes, which only persist for a limited amount of time within the observed scene, may hence be missed in the analysis (Anders et al., 2019) as their timing and/or existence are not known to the analyst and their disappearance is not expressed in later topographic information (Fig. 1A). Performing pairwise change analysis for all combinations of epochs to solve this drawback would be somewhat impractical, and has not been done so far to our knowledge. Pairwise change analysis, therefore, is not adequate to analyse 3D time series for changes that occur with highly varying temporal characteristics, that is timing, change rate, duration of change processes, and persistence of change forms. Surface changes further occur at varying spatial scales regarding their extent, shape and magnitude and can therefore not be extracted generically with one-for-all settings. Where morphologic boundaries of objects or forms moreover are not distinct, it is difficult to spatially delineate them in individual scenes. Binary surface change information (change/no change) has been used to identify and delineate so-called change objects (Liu et al., 2010). However, these spatially contiguous areas of surface change do not necessarily stem from the same change-inducing process (Fig. 1B). Separating them into individual objects without a priori knowledge or information on external influences is improved when integrating the history of surface change that is contained in the 3D time series in the analysis (Anders et al., 2020b).

Time series clustering (Kuschnerus et al., 2020) has been proposed for extracting change information from large 4D geospatial data. The method is useful to extract areas that are homogenous in their change dynamics and thereby finding dominant change patterns in the observed scene. It is not possible, though, to identify individual, spatially and temporally limited change occurrences as the full time series of the observation period are used as input.

Object extraction by integrating the history of surface change can be performed with the concept of 4D objects-by-change (4D-OBCs; Anders et al., 2020b). This method identifies areas in the scene where the surface changes similarly over time within sub-periods in the time series at neighbouring locations. Sub-periods are automatically detected in the temporal domain of a location and are subsequently used as seeds for spatial region growing with time series similarity as homogeneity criterion. The seed locations at which to perform the temporal change detection have been selected manually so far. However, changes occurring are spatially variable within a scene and their timing and location is in general not known to the analyst. Automatic extraction of

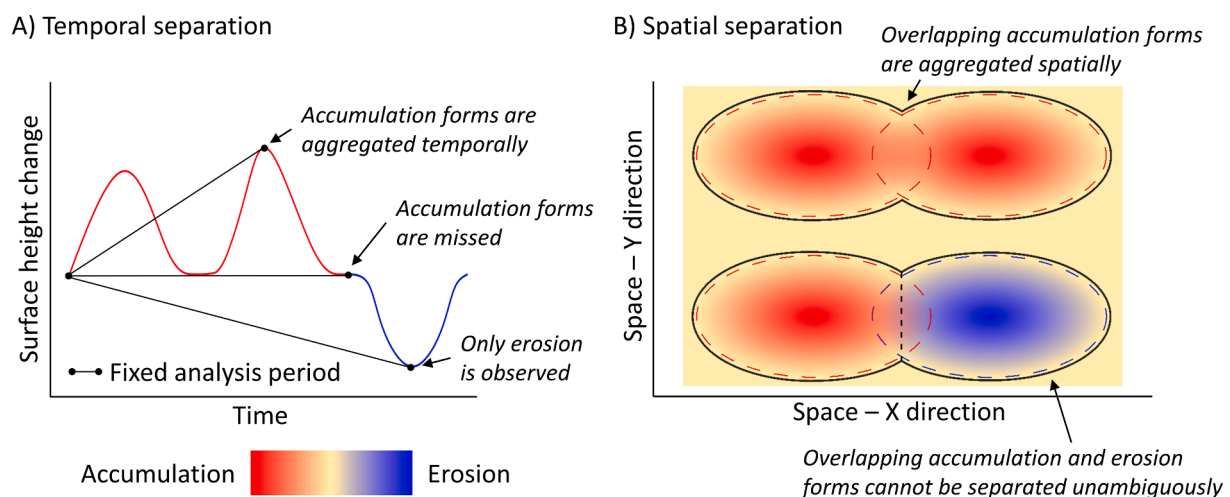


Fig. 1. Spatial and temporal properties of continual surface change in a scene that lead to ambiguity in change information when using pairwise change analysis, but can be resolved by integrating the history of surface change in the analysis. (A) Temporal separation: Individual temporary surface changes may be either missed or aggregated in case of consecutive occurrences when using fixed analysis periods. (B) Spatial separation: Surface changes that overlap spatially and temporally may not be separable into individual forms without considering their spatiotemporal change characteristics.

changes from entire datasets will therefore require fully automatic seed selection from all seed candidates. These can be obtained as sub-periods via temporal change detection at all locations in the scene. Many of these detected sub-periods will be both spatially neighbouring and temporally overlapping, and thereby likely belong to the same change form. One could perform the segmentation for all detected sub-periods at all locations and subsequently aggregate segments into unique 4D-OBCs in a post-processing step. This option is hardly viable, given the large data volumes of 3D time series and considering the extreme redundancy of computations if each location within a change form is used as seed to obtain the same, single object.

The drawbacks outlined above become particularly apparent in settings with continuous surface morphology and dynamic changes of the surface due to material transport induced by varying external drivers. Therefore, the use case of this paper is TLS-based monitoring of a sandy beach, using an hourly time series spanning five months. Sandy beaches are highly active in their morphodynamics through multiple processes acting on the surface, as these coastal landscapes are subject to continual sediment transport by wind, waves, as well as anthropogenic modifications. Their surface is hence shaped by a variety of (temporary) forms of accumulation, erosion, and transported material (Walker et al., 2017). Therefore, the target changes to be extracted from our data are temporary accumulation and erosion forms which typically exist over periods of days to few weeks.

The objective of this paper is to develop a fully automatic workflow to extract surface changes as temporary accumulation or erosion forms in their varying spatial and temporal extents from a long and dense 3D time series dataset. To achieve this, we implement methods of automatic seed selection and locally adaptive thresholding for spatiotemporal segmentation. We consider the following methodological aspects:

- Integrating the history of surface change in temporal change detection will avoid missing temporary surface changes in the analysis which may not persist throughout epochs that are selected for fixed-period analyses.
- Sorting and selecting seeds for region growing by an appropriate metric and considering previous segments throughout continued segmentation allows avoiding redundant calculations but also prevents skipping relevant change occurrences.
- A locally adaptive approach of threshold selection is more suitable than pre-defined thresholds, albeit strict or loose, in order to avoid general over- or underestimation of spatial extents due to dependence on magnitude, duration, and change rate of the respective change form.

The developed automatic spatiotemporal segmentation approach is designed to improve both the spatial separation of change forms, e.g. two co-occurring 4D-OBCs that would otherwise be extracted as one

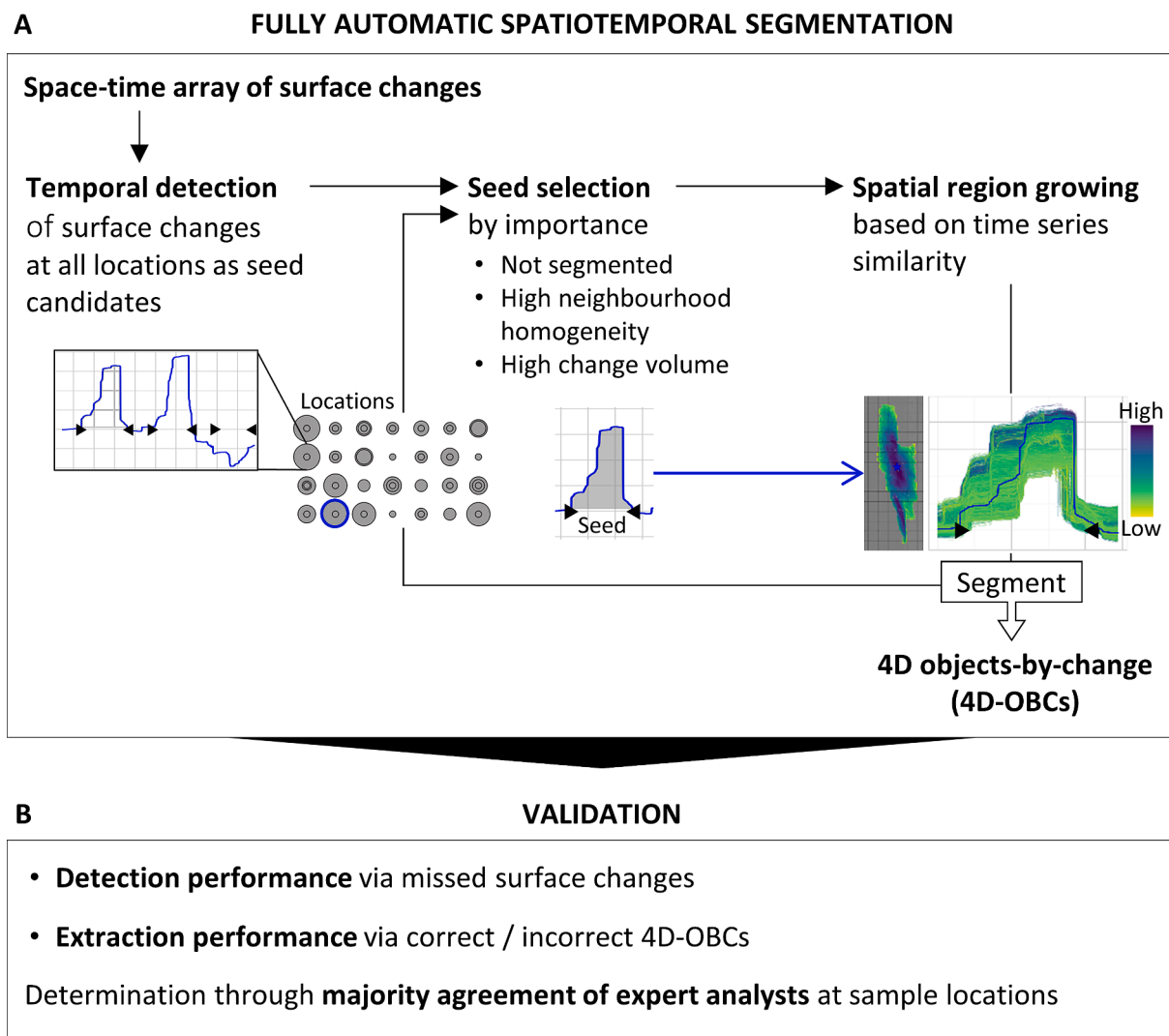


Fig. 2. Overview of the approach to (A) fully automatic spatiotemporal segmentation using a space–time array of surface changes quantified for a 3D time series and (B) validation of results.

accumulation or erosion object, and the temporal separation of change forms, e.g., two consecutive 4D-OBCs that could be aggregated or missed with alternative methods (cf. Fig. 1). Our approach thereby provides an important contribution to the toolset for change analysis in large 4D geospatial data.

2. Data and methods

We use a time series of hourly TLS data with 2,942 epochs acquired at a sandy beach to perform a fully automatic extraction of 4D-OBCs. The results are validated by a group of expert analysts, who assess the detection and extraction performance of our method for sample locations. In addition, we compare extracted 4D-OBCs with changes derived from the baseline method of pairwise change analysis. The main steps of our approach and the investigation of results are visualised in Fig. 2, with details on data and methods outlined in the following sub-sections.

2.1. Data

The 3D time series used in this paper is an hourly dataset of TLS point clouds acquired in the frame of coastal monitoring at the sandy beach of Kijkduin (52°04'14"N, 4°13'10"E; Fig. 3), The Netherlands, over a period of five months (Vos et al., 2017). During the acquisition in the winter season of 2017, a Riegl VZ-2000 (Riegl LMS, 2017) laser scanner was installed in a fixed frame on a hotel building around 30 m above the ground to capture the beach scene below at ranges of 100 to 600 m with resulting point densities of 2–20 points/m². Further details on the observation setup and acquired data can be found in Vos et al. (2017) and Anders et al. (2019).

The analysed dataset has a spatial extent of around 300 m × 600 m and covers the acquisition period from 2017-01-15 to 2017-05-26 with 2,942 epochs. The first epoch is used as reference scan both for iterative closest point (ICP)-based alignment of each epoch using stable planar surfaces in the built-up area between the dunes and the hotel building, and for quantifying surface change for each epoch in the time series via point cloud distance computation. An assessment of alignment accuracy and considering a range-dependent effect of atmospheric conditions on the LiDAR measurements over time yields a minimum detectable change of 0.05 m for this dataset (cf. Anders et al., 2019).

Point cloud distances are obtained using the M3C2 algorithm (Lague

et al., 2013) at locations in a regular grid of 0.5 m spacing, which provides a space–time array of surface change values (Fig. 4). During distance computation, the regular grid locations are used as core points, for which the surface position in both point clouds is averaged using all points in a neighbourhood of 1.0 m radius. To remove change values that are likely to represent measurement errors in single epochs, temporal averaging is applied to each location in the scene by setting surface change values to the median value in a window of one week, i.e. spanning half a week before and after the respective epoch. For further details on the preparation of data, we refer to Anders et al. (2020b).

The space–time array of surface change values is used as input for the methods and all analyses in this paper. The structured dataset provides the 1D time series of surface change at each 2D location along the temporal domain. Each horizontal 2D slice of the array represents surface change for scenes of individual epochs compared to the reference epoch (Fig. 4). The surface change scene of individual epochs corresponds to results provided by fixed-period, pairwise change analysis. A time series of surface change at an example location and surface change in the scene for selected epochs are provided for the dataset in Fig. 5.

2.2. Detection of seed candidates

As a first analysis step, a detection of temporal changes is performed for the time series of all locations in the scene. Change occurrences are detected in the temporal domain using a sliding window approach which determines changes in the median according to the change point detection method presented in Anders et al. (2020b). All detected surface changes with determined location and sub-period, i.e. start and end times of a detected change, are considered seed candidates for spatio-temporal segmentation. For selecting seeds in order of their importance during the full segmentation, the seed candidates are sorted regarding two aspects: First, the similarity of surface change history in their immediate spatial vicinity and, second, their change volume, assuming that higher-magnitude or longer-duration changes are more relevant. The change volume is hence computed as the integral of the absolute surface change over the sub-period of a detected change.

The neighbourhood similarity of surface change history of a seed candidate is obtained as average time series similarity within a detected sub-period in its immediate (3 × 3) spatial neighbourhood, i.e. the mean similarity of the eight neighbour locations. Time series similarity is

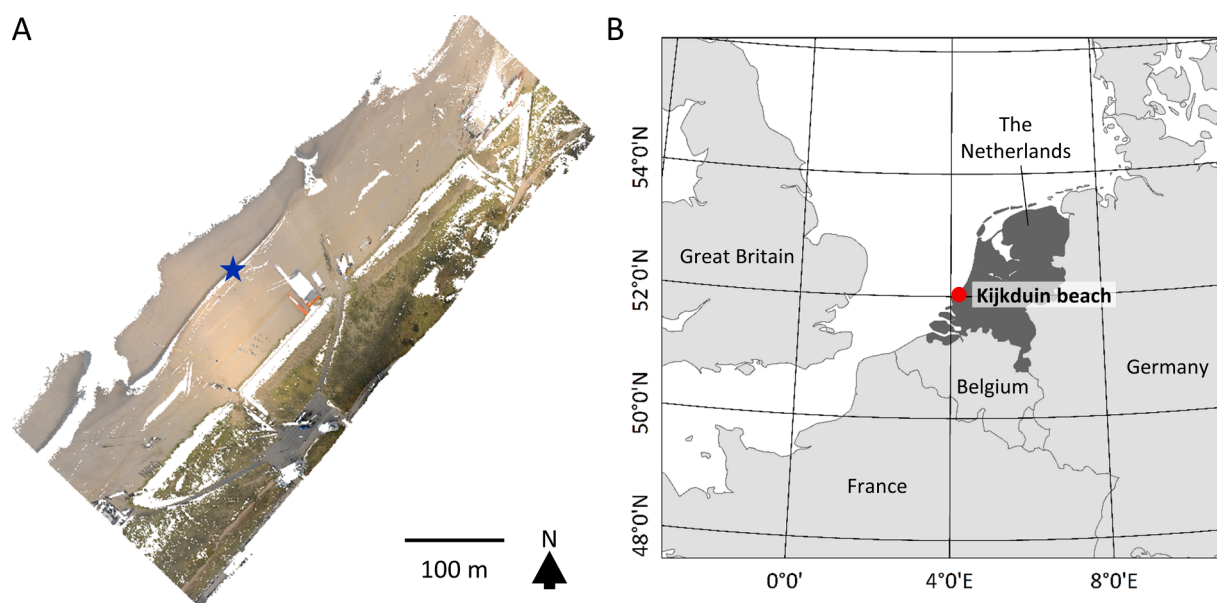


Fig. 3. (A) 3D scene of the sandy beach in Kijkduin (RGB-coloured) and (B) location of the study site in The Netherlands. The star marks the location of the time series of surface change shown in Fig. 5. Data: World Borders © thematicmapping.org 2017.

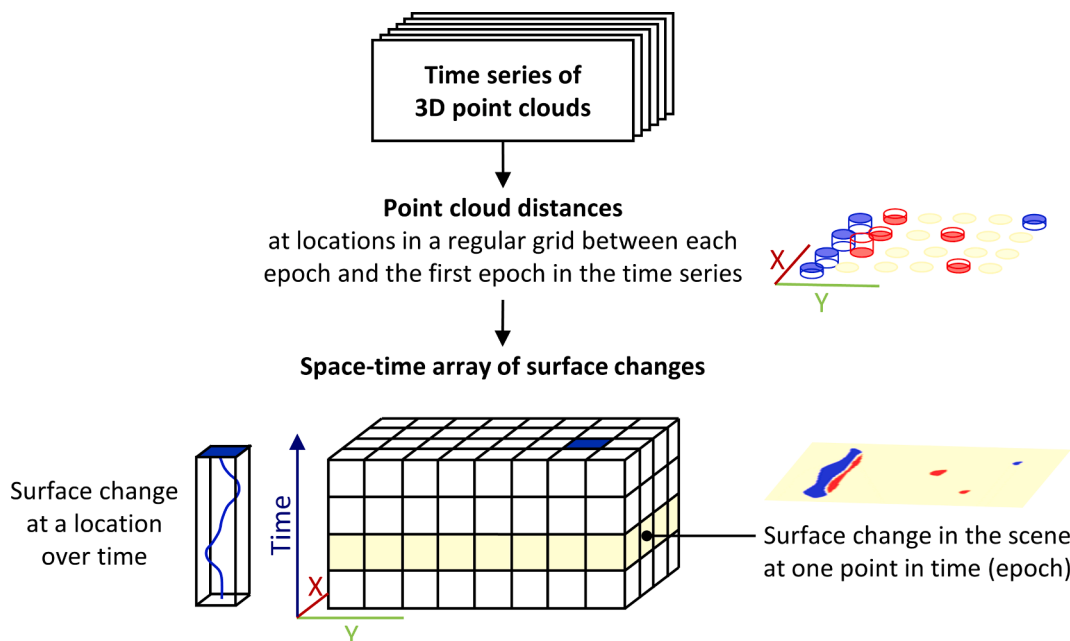


Fig. 4. Schematic of procedure to derive a space–time array of surface changes from a time series of 3D point clouds.

based on Dynamic Time Warping (DTW) distance (Berndt & Clifford, 1994) between a reference and a compared time series. As DTW distance values depend on the magnitude and number of observations in the input time series, we normalise the computed distance D_{abs} based on the maximum possible distance for each reference time series according to the following equation (Eq. (1)):

$$D_{norm} = \min\left(1.0, 1.0 - \frac{D_{max} - D_{abs}}{D_{max}}\right) \in [0, 1] \quad (1)$$

$$\text{with } D_{max} = \int_I |T_{ref}(i) - di| \approx \sum_i |T_{ref,i}|$$

where D_{max} is the maximum possible distance that can result from the comparison, which is derived as the total change volume in the reference time series T_{ref} . If the result of this normalisation is larger than 1.0, the normalised distance D_{norm} is set to the maximum value of 1.0. This can occur, for example, if the reference time series experiences positive change while the compared time series experiences negative change, and means they are highly dissimilar. The normalised DTW distance D_{norm} is considered as direct inverse of time series similarity. It is used to compare seed neighbourhood similarity for obtaining the list of sorted seed candidates as described above. D_{norm} further provides the homogeneity metric in the subsequent region growing, as described in the following section.

2.3. Spatiotemporal segmentation with seed selection and adaptive thresholding

The second analysis step is the actual spatiotemporal segmentation. This is performed via region growing starting from a seed location and using time series similarity at neighbouring locations as homogeneity criterion. Time series similarity is derived from the normalised DTW distance D_{norm} of a compared time series to the seed (Section 2.2). We further adapt the region growing by subtracting the first value of the sub-period from each time series before DTW distance computation. By this, the comparison of surface change values is independent from both the initial surface elevation in the reference epoch and the course of surface changes up to the starting point of the detected change. The latter was lacking in the original version, where the median value of the sub-period was subtracted, which depends on the surface change history

of the detected change itself (cf. Anders et al., 2020b).

2.3.1. Automatic seed selection during segmentation

The segmentation starts with the seed from the top of the list of sorted seed candidates (Section 2.2) and continues with the seed candidate at the next lower rank after concluding region growing of a segment. Seed candidates are omitted if the detected temporary change form is not completed, i.e. does not disappear, up to the end of the time series or if the detected sub-period exceeds a duration of eight weeks. This eight-week maximum duration serves to exclude detected changes that represent signals of larger temporal scales. It is set liberally to cover a third of the observation period of this dataset and does not affect the temporary changes we are aiming at in our use case (cf. Section 1). We further discard seed candidates if the maximum surface change value in the sub-period is below the minimum detectable change, which is determined at 5 cm for this dataset (cf. Anders et al., 2020b).

Finally, seed candidates are also omitted if they were segmented into the 4D-OBC of a previous seed, meaning they are located in the spatial extent of an existent segment and occur in overlapping epochs. The region growing itself is not restricted by previous segments, so that 4D-OBCs may overlap both spatially and temporally. This is adequate for the premise of this paper that surface changes in natural scenes often overlap in their timing and affected area (Section 1). However, for the selection of seeds it can be assumed that the history of surface change in the area of overlap with another 4D-OBC is not the most representative to delineate a potentially additional, superimposed surface change from that seed candidate. If the superimposed surface change is relevant and occurs independently from the previously segmented overlapping 4D-OBC, a suitable seed outside the existent segment is expected to be found in the remainder of the seed candidates.

2.3.2. Automatic thresholding and validity of segments

To spatially delineate surface changes covering a large range of magnitudes and durations within one fully automatic segmentation procedure, robust thresholding is an important aspect of the region growing segmentation. Surface changes with high magnitude and/or long duration will require looser thresholds of time series similarity to delineate the entire object and avoid premature termination, whereas segments with lower change volume are more prone to leakage during the region growing if thresholds are not strict enough. Leaking is here

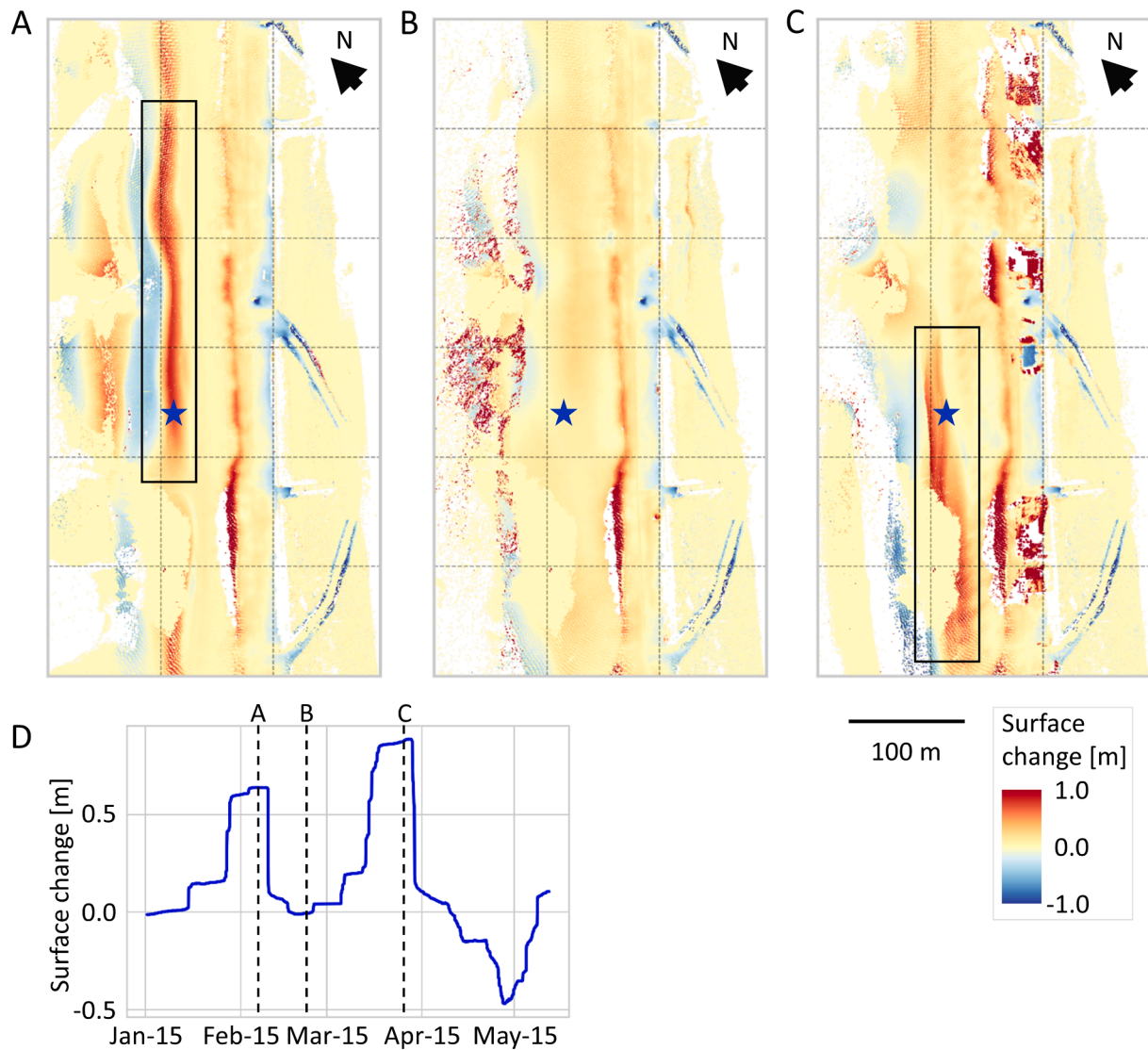


Fig. 5. Surface change on the beach for three selected epochs (A–C) compared to the reference epoch at the beginning of the 3D time series, respectively. The epochs are marked by dashed lines in (D) the time series of surface changes at an example location (marked by star in maps A–C). Surface increases in the time series at this location belong to temporally independent accumulation forms of different spatial extent (boxes in A and C).

referred to the growing of a segment outside the correct spatial extent. There is no one-for-all solution to thresholding and suitable thresholds cannot be determined solely based on the seed properties, as they lack information on the spatial segment properties. We solve this by performing the region growing for a range of thresholds in parallel and deciding for the most suitable version based on the resulting segments. Accordingly, the region growing is performed for normalised DTW distance thresholds of 0.3 to 0.9 in steps of 0.1. We select the most suitable threshold based on the resulting segment sizes which should not change abruptly between thresholds increased or decreased by one step. If the ratio of segment sizes between increasingly large thresholds decreases, it indicates that the segment size strongly increased and it is likely that leakage occurred. The threshold value which produces the first local maximum of segment size ratios for increasing thresholds is therefore used to provide the final result of the segmentation.

Before continuing segmentation, a resulting segment is checked for its validity. Segments are discarded as invalid if they exceed a certain level of within-segment heterogeneity. For this purpose, heterogeneity is derived as coefficient of variation (CV, Eq. (2)) of the change volume at all locations in the segment.

$$CV = \frac{\sigma}{\mu} \tag{2}$$

where σ is the standard deviation and μ the mean of values at all locations in a segment. The CV value indicates variability of surface change histories within the segment and was found to be most suitable in an exploration of selected valid and non-valid segments. The threshold was thereby determined at a $CV \leq 0.8$ of normalised DTW distances for segments to be accepted as valid. All segments obtained in this way are used to determine the spatiotemporal overlap for subsequent seed candidates, which are skipped if already segmented (Section 2.3.1). Regarding the extraction of 4D-OBCs, ultimately, only segments with a minimum segment size of 10 locations (i.e., 2.25 m²) are used as result for the use case of this sandy beach (cf. Anders et al., 2020b).

We check the suitability of the automatic thresholding based on evaluations provided by expert analysts in the validation, which is presented in the following section.

2.4. Evaluation of results

The performance of the fully automatic segmentation is assessed

regarding both the detection of surface changes and their spatial delineation as 4D-OBCs. The detection performance is particularly important to assess, as it is not possible to procure the ground truth of all changes that occur during an observation period. We hence choose a validation approach common to detection tasks in remote sensing, using reference data generated by a group of human interpreters who check the data and results at a number of locations in the area of interest (e.g., Foga et al., 2017; Healey et al., 2018).

The group of interpreters are six analysts with expertise in 3D change analysis. Each analyst evaluates the segmentation performance at 72 evenly distributed locations in the scene. At each validation location, the detection performance is assessed based on the 1D time series of surface changes and an animation of surface changes in the area of that location, so that the analyst can identify change occurrences that are not segmented in any 4D-OBC. The analysts further decide on the correctness of each 4D-OBC that was extracted at a validation location, meaning the location is included in the spatial extent of an object. Objects that cannot be recognized as suitable surface change information by the analysts are marked as incorrect. Objects identified as suitable may be designated as fully correct, or too large or small in spatial extent.

To account for subjective errors in the complex task of evaluating extracted surface changes, we use majority aggregation of expert results for each location and object (Herfort et al., 2018). Accordingly, more than 50% of experts need to mark a change as being missed to result in a false negative (FN) or an object as being incorrect to result in a false

positive (FP). Objects that are correct according to the majority aggregation are true positives (TP).

From these reference data, we validate our results using the error of omission (Eq. (3)) and the error of commission (Eq. (4)):

$$\text{Error of omission} : \frac{FN}{FN + TP} \tag{3}$$

$$\text{Error of commission} : \frac{FP}{FP + TP} \tag{4}$$

We discuss the performance of our method based on this evaluation and for representative 4D objects-by-change resulting from the fully automatic spatiotemporal segmentation. The material used for validation and results of the expert evaluation are openly available in the data repository of Heidelberg University (Anders et al., 2021).

3. Results

In the spatial–temporal extent of the dataset, a total of 306,728 surface changes are detected as sub-periods at 192,901 locations in the scene, which derive from over 15 billion LiDAR points in the full 3D time series. The detected sub-periods are sorted by decreasing neighbourhood similarity and therein decreasing change volume, and provide the seed candidates for the segmentation (Section 2.2). A total of 7,893 segments are generated by the full segmentation until the end of the seed

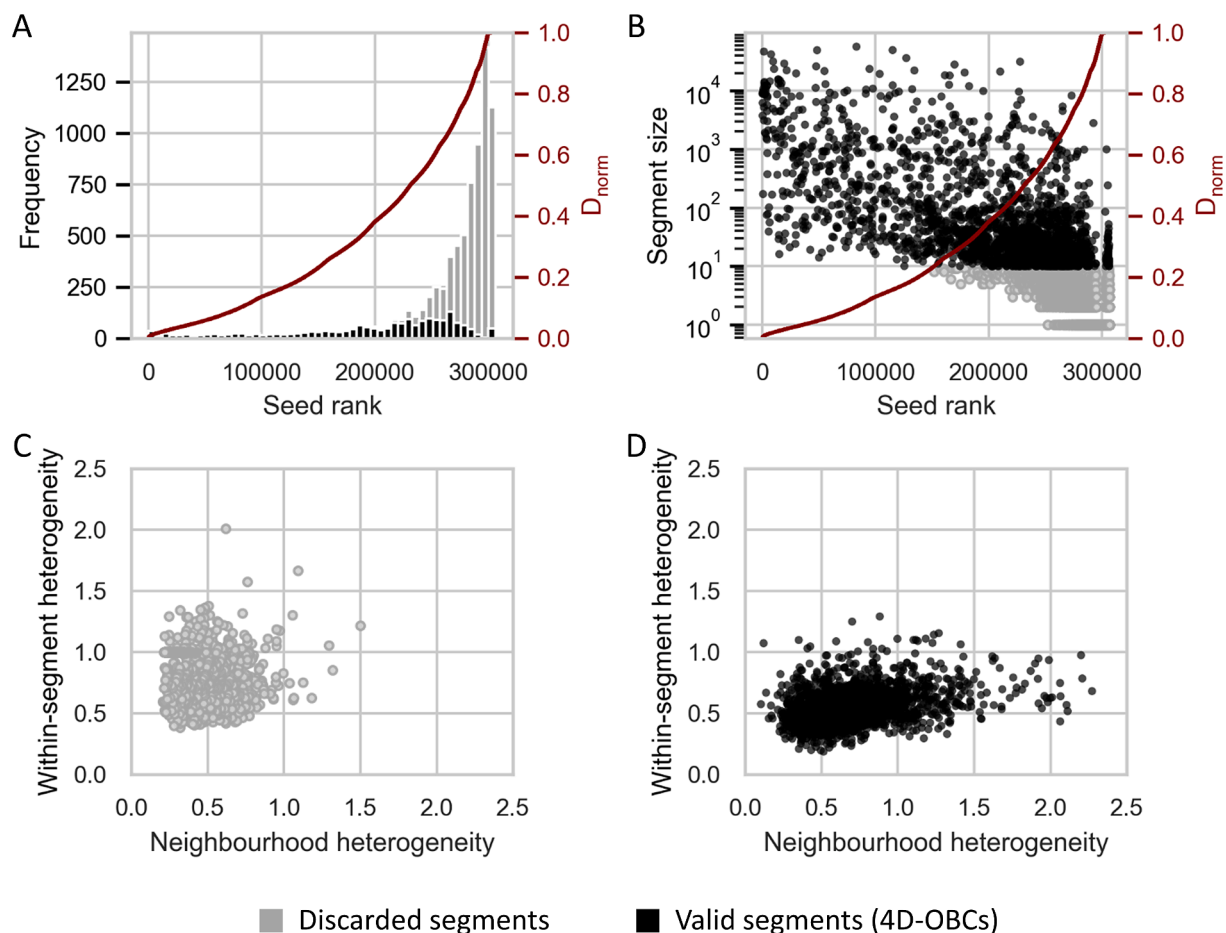


Fig. 6. Seed and segment properties in relation to the full list of seed candidates, and compared by valid and discarded segments. Seed candidates are sorted by normalised DTW distance D_{norm} as metric of inverse neighbourhood similarity. (A) Frequency of seeds in the range of sorted seed candidates shows a strong increase in the number of segments towards the end of the candidate list. (B) Segment sizes show a strong overall decrease at the end of the candidate list. Segment size is the number of segmented locations, note that the axis of segment size is logarithmic. Bottom row shows the relation of seed neighbourhood heterogeneity to within-segment heterogeneity as coefficient of variation (CV) of normalised DTW distances D_{norm} for (C) discarded and (D) valid segments. Segments are invalid (grey) if their segment size is below the minimum size or the change volume of time series at all locations in the segment is very heterogeneous.

candidate list. Invalid segments are determined by the criteria of inner-segment heterogeneity (59 segments discarded) and minimum segment size (5,813 segments discarded). In consequence, 2,021 segments are designated valid and provide the final result of 4D-OBC extraction.

3.1. Seed sorting and selection

The distribution of seeds used for segmentation over the full list of sorted seed candidates (Fig. 6A) shows that increasing numbers of seeds are selected towards the end of the candidate list. This indicates that less seed candidates are skipped with ongoing segmentation, and therein decreasing neighbourhood similarity of sorted candidates. At the same time, seeds towards the end of the candidate list result in overall much smaller segment sizes (Fig. 6B), which are mostly discarded by the minimum size criterion (coloured in grey in Fig. 6; cf. Section 2.3.2). More than half of these discarded segments (3,059 of 5,813) only consist of the seed location itself (segment size of 1), another 27% have a size of only 2–3 locations. Even for the loosest of thresholds (0.9) of the parallel runs, no real segment is grown for these seeds, which are mostly spatially isolated locations, for example in areas of sparse data due to occlusion or water influence.

Segment sizes at the beginning of the seed list are overall larger and highly variable. The latter fits the nature of surface changes that may occur at a large range of spatial extents. This result demonstrates that seeds with lower importance in the sense of neighbourhood similarity lead to fewer meaningful 4D-OBCs, or, put the other way round, lead to more segments that should be discarded.

The suitability of this validity criterion is demonstrated in the relation of seed neighbourhood heterogeneity to within-segment heterogeneity (Fig. 6C and D). Heterogeneity is derived as coefficient of variation CV (Eq. (2)) of time series similarities D_{norm} , respectively, for neighbourhood heterogeneity in the seed neighbourhood, and for within-segment heterogeneity for all locations in the segment. In contrast to valid segments that are considered as final 4D-OBCs, discarded segments show particularly high within-segment heterogeneity even though their neighbourhood heterogeneity is comparably low.

3.2. Validation of spatiotemporal segmentation results

A total of 107 4D-OBCs, which extend over 38 of 72 validation locations, were extracted for evaluation through experts. At the other locations no changes were detected or segments are discarded as invalid. Since some 4D-OBCs cover multiple validation locations in their spatial extent, the expert analysts provide 169 object assessments for the total of evaluated locations. Results of expert evaluations are aggregated by majority agreement of all six analysts for each location and 4D-OBC, respectively (Table 1).

According to the expert validation, the error of omission regarding missed surface changes amounts to 4.7%. The error of commission

Table 1

Aggregated evaluations by six expert analysts for 169 objects at 72 validation locations. Correct 4D-OBCs are true positives (TP), incorrect 4D-OBCs are false positives (FP), and missing 4D-OBCs represent false negatives (FN). Percentages for these missed surface changes are not available, as there is no quantification of true negatives.

Final evaluation	Expert evaluation	Number	Percentage
Correct 4D-OBCs		141	83%
	<i>Fully correct</i>	98	58%
	<i>Too small</i>	21	12%
	<i>Too large</i>	22	13%
Incorrect 4D-OBCs		28	17%
	<i>Weird/cannot specify</i>	10	6%
	<i>Incorrect</i>	18	11%
Missing 4D-OBCs	<i>Missed surface change</i>	7	–

regarding the number of incorrectly extracted 4D-OBCs amounts to 16.6%. Of the 83% true positives, 58% of objects were marked as fully correct, whereas 12% and 13% were evaluated as too small and too large in their spatial extent, respectively. We check these evaluations in the subsequent section regarding locally adaptive region growing thresholds for specific 4D-OBCs.

3.3. Automatic thresholding and extracted 4D objects-by-change

The region growing threshold for spatiotemporal segmentation is automatically determined for each seed based on the resulting segments for a set of thresholds (cf. Section 2.3.2). This avoids general over- or underestimation of spatial extents for change forms with differing properties in the variety of magnitudes and durations of surface changes. In most cases, a normalised DTW distance threshold of 0.4 or 0.5 is selected for the region growing of 4D-OBCs (1,284 of 2,021 valid segments). A decreasing number of 4D-OBCs is extracted with looser region growing thresholds, with the lowest number of 47 objects extracted with a distance threshold of 0.9. Descriptive statistics of thresholds are listed in Table 2.

In some cases, the automatic threshold selection does not perform ideally, which is demonstrated by the expert evaluations of extracted 4D-OBCs being too small or too large in spatial extent (cf. Section 3.2). Subsequently, we show two representative examples why this occurs with the developed approach of locally adaptive thresholding.

The threshold selection is designed to avoid strong increases of segment sizes for small increases of the region growing threshold. In some cases, this causes the spatial extent to only cover a fraction of the actual change form. This occurs mostly if there are gaps in the topographic information or low point densities, for our data particularly in the outer beach area that is strongly and frequently influenced by water (Fig. 7A and C).

In the same example 4D-OBC, the automatic thresholding prevents the segment from being delineated extremely large for an even looser threshold (Fig. 7B). The accumulation form is extracted with another 4D-OBC in its correct spatial extent using a seed that is ranked a few positions after this example object. Thereby, the change form as a whole is not missed, since a more suitable seed for delineation is available later in the list of seed candidates. An important aspect for using results of the spatiotemporal segmentation for subsequent analysis will therefore be to filter or aggregate potentially superfluous objects that cover the same change form but do not correctly represent its spatial extent.

In contrast to undersized objects which can be extracted correctly by additional seeds at a progressed stage of the segmentation, there are 4D-OBCs which are evaluated as too large. These cases occur if the segments resulting from the strictest possible region growing threshold already produce oversized segment sizes (Fig. 8). Subsequent seed candidates representing the same change form are not used for region growing if they are already segmented in the area of the oversized object and a more suitable extraction as 4D-OBC will hence not be available. A relevant change form is nonetheless detected and extracted by these 4D-OBCs with overestimated spatial extent. For subsequent analysis, a postprocessing step would allow to refine the spatial delineation of such cases. A potential issue that should be taken into account regarding the full spatiotemporal segmentation, is that the spatial extent of oversized segments potentially incorporates other change forms that would not be

Table 2

Number of segments and statistics of final segmentation threshold for all segments and only valid segments. Possible thresholds of normalised DTW distance range from 0.3 to 0.9.

Segments	Number	Final segmentation threshold (time series similarity)				
		Mean	Median	Std. dev.	5th Perc.	95th Perc.
All	7,893	0.45	0.40	0.09	0.40	0.60
Valid	2,021	0.53	0.50	0.12	0.40	0.80

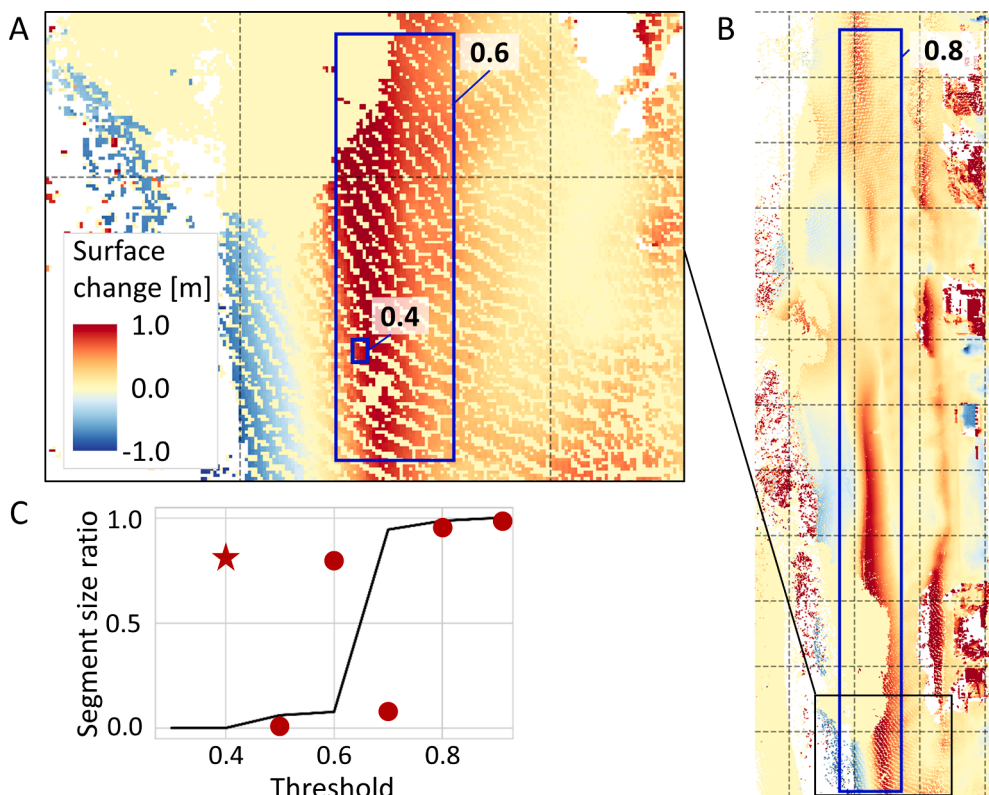


Fig. 7. Result of segmentation for 4D object-by-change that was evaluated as too small in the expert-based validation. The method of automatic thresholding determines a strict normalised DTW distance threshold of 0.4 time series similarity at the maximum segment size ratio before decreasing for a higher threshold (marked by red star in C). (A) Spatial extent of the segment for the selected threshold of 0.4 as well as a looser threshold of 0.6, which would be more suitable in the case of this change form. The bounding box in (B) illustrates the segment resulting for an even looser threshold of 0.8, which leads to a large portion of the beach being segmented for this detected accumulation form and is prevented by the locally adaptive thresholding method. (C) Segment size ratios for each region growing threshold in relation to the largest segment size (black line) and to the segment size of the next-stricter threshold (red dots, red star marks selected threshold). Grid spacing of maps is 25 m. (For interpretation of the references to colour in this figure legend, the reader is referred to the web version of this article.)

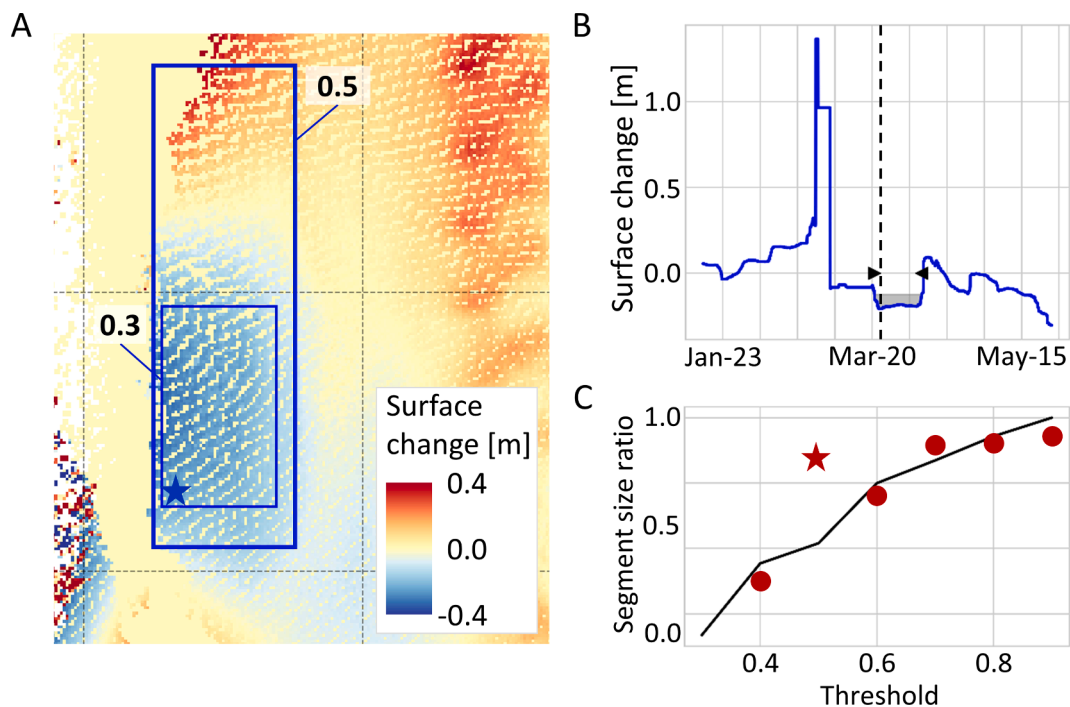


Fig. 8. Result of segmentation for 4D object-by-change that was evaluated as too large in the expert-based validation. (A) Spatial extent of the segment for the selected normalised DTW distance threshold of 0.5 as well as the strictest threshold computed in the full segmentation of 0.3, which would be more correct in the case of this change form. The strictest possible threshold (given the ratio-based selection method) is 0.4, for which the overestimation of the spatial extent already occurs. The detected surface change has a low magnitude in relation to a long duration, which is visualised in the time series of the seed location in B (start and end point of the detected temporal change marked by arrows, location marked by star in A). (C) Segment size ratios for each region growing threshold in relation to the largest segment size (black line) and to the segment size of the next-stricter threshold (red dots, red star marks selected threshold). Grid spacing of map is 25 m, the epoch is marked by the dashed line in B. (For interpretation of the references to colour in this figure legend, the reader is referred to the web version of this article.)

possible to extract anymore due to the design of seed selection, i.e. skipping seed candidates that are segmented in a previous object (Section 2.3.1). To our best knowledge, this does not occur for our use case of full spatiotemporal segmentation. We further consider this unlikely to be a general issue, since spatial extents being too large due to the described cause mainly occurs for subtle change forms with low magnitude in relation to longer durations (Fig. 8B). These will not grow into the area of other relevant surface changes given the homogeneity criterion of time series similarity.

3.4. Improvement of surface change extraction using spatiotemporal segmentation

Spatiotemporal segmentation is a method of time series-based change analysis with the objective to avoid both missing changes due to fixed-period analysis and aggregating spatially and/or temporally overlapping surface changes, which can occur in pairwise change analysis (cf. Fig. 1). We demonstrate how this is overcome through the extraction of 4D-OBCs with an example of an accumulation form and an erosion form co-occurring during the same period and in adjacent spatial extents. The same accumulation form spatially overlaps with another accumulation form that occurs in a successive, temporally independent period (Fig. 9).

The spatial extents of the accumulation and erosion form demonstrate that each surface change is delineated regarding its surface change history and independently of the border of another, simultaneously occurring change form (Fig. 9A and C, marked by 1 and 2). Importantly, this further visualises how the time series-based analysis is not affected by the selection of the reference epoch used for bitemporal change quantification. The detection and delineation of accumulation and erosion in fixed-period analyses relies on the sign of surface change values, and the selection of epochs determines the magnitude, and, critically, the direction of changes in the resulting bitemporal change image. When considering the surface change history, change forms will

be identified as positive or negative surface changes irrespective of the signed surface change values (Fig. 9C).

4. Discussion

The ability to identify and separate individual change forms spatially and temporally with time series-based change analysis is an important improvement regarding drawbacks of standard pairwise change analysis approaches (cf. Section 1). The change analysis becomes independent of selecting analysis periods and also of selecting a reference epoch that most suitably represents the initial state of the surface, relative to which accumulation and erosion are determined. Particularly in natural scenes characterised by complex, multidirectional morphodynamics, such as the surface of a sandy beach in coastal monitoring, acquisitions of some initial state of the terrain are usually not available. In our use case, we follow the common approach of using the first epoch of the data as reference for bitemporal change quantification. This has no effect on the method of spatiotemporal segmentation, which is based on the history of surface change rather than signed surface change values.

With our developed approach of fully automatic extraction of 4D-OBCs from a 3D time series, we are able to extract temporary accumulation and erosion forms with a completeness of around 95% according to reference data at 72 locations in the scene (error of omission of 4.7%, Section 3.2). To our knowledge, there is currently no method capable of equivalent generic detection of surface changes from 3D time series to compare the performance of our method to. Our approach achieves a similar performance as is reported for detection and extraction tasks from time series of satellite images, such as mapping of burned areas with detection of seed pixels and subsequent region growing (error of omission of 10–16%; e.g. Bastarrika et al., 2011) or a time series-based change detection method for land cover change (overall accuracy of 88%; e.g. Lin et al., 2019). The error of commission amounts to 16.6% due to a few incorrectly extracted objects. Filtering out these segments which are not useful as 4D-OBCs could be integrated in subsequent

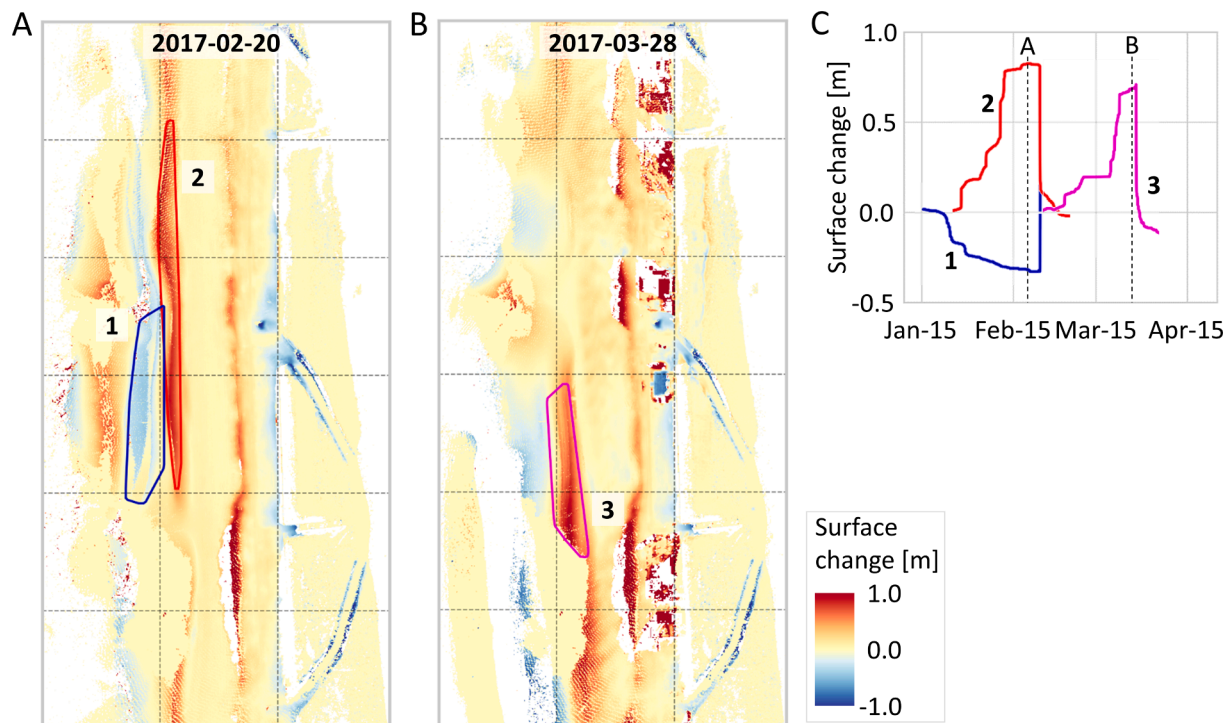


Fig. 9. 4D objects-by-change (4D-OBCs) of an erosion form (1) and two accumulation forms (2 and 3) whose spatial extent is depicted in surface change maps (A and B) of the full scene at the epochs of their highest magnitude, respectively. (C) Time series of surface change of the three temporary change forms (1–3) throughout the period of their existence. Time series show the surface change at the seed location of each 4D-OBC. Dashed lines mark the epochs of maps A and B. Grid spacing of maps is 100 m.

processing steps. Using (only) segments with specific properties for identification of target objects or classification in scenes is an integral part of object-based analyses (e.g., [Mayr et al., 2017](#)).

The developed approach of locally adaptive thresholding enables spatial delineation of surface changes that is flexible to the properties of detected change forms ([Section 3.3](#)). Leakage of segments in the region growing is avoided without the need to introduce threshold criteria tailored to any specific change properties, such as distinguishing between high- and low-magnitude changes for region growing. With this, few parameters are required to apply the methodological workflow. Besides the definition of changes to detect, in our case temporary accumulation and erosion forms, we parametrise the segmentation regarding (i) limitations of our dataset, i.e. the minimum detectable change, and (ii) a priori information on target changes, i.e. a maximum duration of surface changes to be considered (cf. [Section 2.3.1](#)). Adjusting or leaving out these settings would mainly influence the number of 4D-OBCs that are extracted and potentially require more careful selection of appropriate objects for subsequent analysis.

Postprocessing of segments should further regard aggregation of single 4D-OBCs that represent the same change form. In particular, this can occur if objects are undersized. Their area then does not cover the full spatial extent of a change form and another seed can be found for region growing in the remaining list of seed candidates. This affects around 15% of extracted 4D-OBCs ([Section 3.2](#)) and mostly occurs in areas where gaps are present in the topographic data, for example due to occlusion or laser shot dropouts caused by water influence ([Höfle et al., 2009](#)). The seed of such an object may therefore qualify as the most suitable regarding the neighbourhood similarity criterion ([Section 2.3.1](#)) but will perform poorly in the region growing with strict thresholds due to a high degree of noise in the extended spatial neighbourhood. Our examination of results indicates that this does not necessarily adversely affect the full segmentation, as a correct 4D-OBC is provided by another seed that is found in the remainder of the seed candidate list (cf. [Section 3.3](#)). An alternative to avoid this would be to include spatial interpolation of surface changes in each epoch of the space–time array during preparation of the input data. The pre- or postprocessing applied to the data and obtained segments, respectively, will typically be tailored to the specific analysis or research question of a use case.

With regards to delineating 4D-OBCs too large in their spatial extent, the design of our method might lead to change forms not being segmented at all if they were incorporated by a previous oversized object and all potential seed candidates are subsequently skipped as segmented. While our results show no indication of such a case, this consideration becomes relevant for the analysis of coinciding change processes. Scenarios where some change form occurs within a larger area of surface change become ever more likely when observation periods cover multiple seasons and years, and the types of surface changes to be extracted by spatiotemporal segmentation are extended in their variety. These could for example be changes to individual morphologic components on top of continual surface lowering, such as the movement of boulders within the creep of a rock glacier ([Ulrich et al., 2021](#)). Accounting for this will require a multiscale approach particularly in the temporal change detection, to separate, e.g., changes at slower rates from simultaneous, spatially overlapping changes.

The presented approach of 4D change extraction works on change information from time series of 3D geodata in a regular structure. The input for the method could hence also be a series of gridded topographic information, such as Digital Elevation Models. The epochs of time series need not be sampled at regular intervals, as is often the case for archives of topographic data. Irregularly sampled time series will require additional considerations, though, for example by weighting epochs in the computation of time series similarity. Alternatively, gaps in the temporal domain of data could be filled by interpolating changes heuristically or based on modelling. Depending on the relation of temporal resolution and length of time series, this could lead to extremely large

data volumes and consequently strongly increased computational cost of spatiotemporal segmentation. The DTW distance computation during region growing is the main factor of computation time with a complexity of $O(es)$, where e is the number of epochs in the sub-period of a detected change and s is the segment size, i.e. the number of DTW distance computations performed. Considering the linear increase of computational cost, analysis could benefit from a reduction in spatial and temporal resolutions, though the influence on extracted 4D-OBCs requires investigation. Ultimately, one can always make use of the original, in case of gridded point cloud data, full 3D information in the spatial–temporal extent of resulting 4D-OBCs to enrich the detail analysis of individual change forms and processes. To reach this point in the analysis, fully automatic spatiotemporal segmentation provides an essential step to detect and extract surface change from large 4D geospatial data.

5. Conclusion

In this paper, we present a fully automatic approach to change analysis from 3D time series data. The method detects changes in the time series at locations in a scene and makes use of spatiotemporal segmentation to delineate change forms. This enables the extraction of 4D objects-by-change (4D-OBCs), i.e. temporary surface changes induced by material transport on continuous surface morphology that are difficult to detect in space and time using single topographic snapshots or fixed-period pairwise change analysis.

The crucial steps to deploy spatiotemporal segmentation for the extraction of changes from 4D geospatial data are the automatic detection of relevant change occurrences, selection of suitable seeds and locally adaptive thresholding of the region growing segmentation that accounts for the variety of spatial and temporal scales that are covered by surface changes in natural scenes. Our developed method of automatic seed detection and selection sorts seeds by their importance for the delineation of individual change forms. It hence avoids highly redundant computation and thereby reduces the segmentation effort. The segmentation from a selected seed itself performs region growing for a set of thresholds in parallel. Through locally adaptive thresholding no decision for one threshold is required. This avoids general over- and underestimation in the spatial extents of 4D-OBCs, which would occur for the variety of magnitudes and durations of surface changes if using a one-for-all threshold of time series similarity during region growing, albeit strict or loose. All in all, a high accuracy is achieved for the detection and delineation of surface changes from the 3D time series dataset.

The extraction of 4D-OBCs from 3D time series improves standard, pairwise approaches to change analysis by removing the requirement to select periods for the analysis of changes. The consideration of surface change histories in the time series-based approach enables the separation of spatially overlapping changes, which might be aggregated in the extraction of accumulation or erosion forms from bitemporal change information of a scene. The developed approach thereby enables a generic extraction of surface changes in their varying spatial and temporal extents from large and dense 4D geospatial data.

6. Data statement

The Python scripts to perform the spatiotemporal segmentation are published openly together with material and results of the validation in the data repository of Heidelberg University (<https://doi.org/10.11588/data/4HJHAA>). The 3D time series data used in this article are available upon reasonable request to S.E. Vos (s.e.vos@tudelft.nl).

Declaration of Competing Interest

The authors declare that they have no known competing financial interests or personal relationships that could have appeared to influence the work reported in this paper.

Acknowledgements

We are greatly thankful to six colleagues who took the time to perform the evaluation of results for validation of the method. This work was supported in part by the Heidelberg Graduate School of Mathematical and Computational Methods for the Sciences (HGS MathComp), founded by DFG grant GSC 220 in the German Universities Excellence Initiative. The acquisition of the TLS time series data was financed by the ERC Advanced Grant Neashore Monitoring and Modeling (grant number 291206) and by the CoastScan project in the NWO Open Technology Programme (grant number 16352). We thank three anonymous reviewers for their comments to improve our paper.

References

- Abellán, A., Calvet, J., Vilaplana, J.M., Blanchard, J., 2010. Detection and spatial prediction of rockfalls by means of terrestrial laser scanner monitoring. *Geomorphology* 119 (3), 162–171. <https://doi.org/10.1016/j.geomorph.2010.03.016>.
- Anders, K., Lindenbergh, R.C., Vos, S.E., Mara, H., de Vries, S., Höfle, B., 2019. High-frequency 3D geomorphic observation using hourly terrestrial laser scanning data of a sandy beach. *ISPRS Ann. Photogramm. Remote Sens. Spatial Inf. Sci.* IV-2/W5, 317–324. <https://doi.org/10.5194/isprs-annals-iv-2-w5-317-2019>.
- Anders, K., Marx, S., Boike, J., Herfort, B., Wilcox, E.J., Langer, M., Marsh, P., Höfle, B., 2020a. Multitemporal terrestrial laser scanning point clouds for thaw subsidence observation at Arctic permafrost monitoring sites. *Earth Surf. Process. Landforms* 45 (7), 1589–1600. <https://doi.org/10.1002/esp.4833>.
- Anders, K., Winiwarter, L., Lindenbergh, R., Williams, J.G., Vos, S.E., Höfle, B., 2020b. 4D objects-by-change: Spatiotemporal segmentation of geomorphic surface change from LiDAR time series. *ISPRS J. Photogramm. Remote Sens.* 159, 352–363. <https://doi.org/10.1016/j.isprsjprs.2019.11.025>.
- Anders, K., Winiwarter, L., Mara, H., Lindenbergh, R., Vos, S.E., Höfle, B., 2021. Fully automatic spatiotemporal segmentation of 3D LiDAR time series for the extraction of natural surface changes [Source Code, Validation Material and Validation Results]. *heidata*, V1. doi: [10.11588/data/4HJHAA](https://doi.org/10.11588/data/4HJHAA).
- Bastarrika, A., Chuvieco, E., Martín, M.P., 2011. Mapping burned areas from Landsat TM/ETM+ data with a two-phase algorithm: Balancing omission and commission errors. *Remote Sens. Environ.* 115 (4), 1003–1012. <https://doi.org/10.1016/j.rse.2010.12.005>.
- Berndt, D.J., Clifford, J., 1994. Using dynamic time warping to find patterns in time series. *AAAI-94 Workshop Knowledge Discov. Databases* 10 (16), 359–370.
- Bodin, X., Thibert, E., Sanchez, O., Rabatel, A., Jaillet, S., 2018. Multi-annual kinematics of an active rock glacier quantified from very high-resolution DEMs: An application case in the French Alps. *Remote Sens.* 10 (4) <https://doi.org/10.3390/rs10040547>.
- Eitel, J.U.H., Höfle, B., Vierling, L.A., Abellán, A., Asner, G.P., Deems, J.S., Glennie, C.L., Joerg, P.C., LeWinter, A.L., Magney, T.S., Mandlbürger, G., Morton, D.C., Müller, J., Vierling, K.T., 2016. Beyond 3-D: The new spectrum of lidar applications for earth and ecological sciences. *Remote Sens. Environ.* 186, 372–392. <https://doi.org/10.1016/j.rse.2016.08.018>.
- Eltner, A., Kaiser, A., Abellán, A., Schindewolf, M., 2017. Time lapse structure-from-motion photogrammetry for continuous geomorphic monitoring. *Earth Surf. Proc. Land.* 42, 2240–2253. <https://doi.org/10.1002/esp.4178>.
- Fabbri, S., Giambastiani, B.M.S., Sisti, F., Scarelli, F., Gabbianelli, G., 2017. Geomorphological analysis and classification of foredune ridges based on Terrestrial Laser Scanning (TLS) technology. *Geomorphology* 295, 436–451. <https://doi.org/10.1016/j.geomorph.2017.08.003>.
- Fey, C., Schattan, P., Helfricht, K., Schöber, J., 2019. A compilation of multi-temporal TLS snow depth distribution maps at the Weisssee snow research site (Kaunertal, Austria). *Water Resour. Res.* 55 (6), 5154–5164. <https://doi.org/10.1029/2019wr024788>.
- Foga, S., Scaramuzza, P.L., Guo, S., Zhu, Z., Dille, R.D., Beckmann, T., Schmidt, G.L., Dwyer, J.L., Joseph Hughes, M., Laue, B., 2017. Cloud detection algorithm comparison and validation for operational Landsat data products. *Remote Sens. Environ.* 194, 379–390. <https://doi.org/10.1016/j.rse.2017.03.026>.
- Girardeau-Montaut, D., Roux, M., Marc, R., Thibault, G., 2005. Change detection on points cloud data acquired with a ground laser scanner. In: *Proceedings of the ISPRS Workshop Laser Scanning 2005*, pp. 30–35.
- Grünwald, T., Schirmer, M., Mott, R., Lehning, M., 2010. Spatial and temporal variability of snow depth and ablation rates in a small mountain catchment. *The Cryosphere* 4 (2), 215–225. <https://doi.org/10.5194/tc-4-215-2010>.
- Healey, S.P., Cohen, W.B., Yang, Z., Kenneth Brewer, C., Brooks, E.B., Gorelick, N., Hernandez, A.J., Huang, C., Joseph Hughes, M., Kennedy, R.E., Loveland, T.R., Moisen, G.G., Schroeder, T.A., Stehman, S.V., Vogelmann, J.E., Woodcock, C.E., Yang, L., Zhu, Z., 2018. Mapping forest change using stacked generalization: An ensemble approach. *Remote Sens. Environ.* 204, 717–728. <https://doi.org/10.1016/j.rse.2017.09.029>.
- Herfort, B., Höfle, B., Klöner, C., 2018. 3D micro-mapping: Towards assessing the quality of crowdsourcing to support 3D point cloud analysis. *ISPRS J. Photogramm. Remote Sens.* 137, 73–83. <https://doi.org/10.1016/j.isprsjprs.2018.01.009>.
- Höfle, B., Vetter, M., Pfeifer, N., Mandlbürger, G., Stötter, J., 2009. Water surface mapping from airborne laser scanning using signal intensity and elevation data. *Earth Surf. Proc. Land.* 34 (12), 1635–1649. <https://doi.org/10.1002/esp.1853>.
- James, L.A., Hodgson, M.E., Ghoshal, S., Latiolais, M.M., 2012. Geomorphic change detection using historic maps and DEM differencing: The temporal dimension of geospatial analysis. *Geomorphology* 137 (1), 181–198. <https://doi.org/10.1016/j.geomorph.2010.10.039>.
- Kromer, R.A., Abellán, A., Hutchinson, D.J., Lato, M., Chanut, M.-A., Dubois, L., Jaboyedoff, M., 2017. Automated terrestrial laser scanning with near real-time change detection – Monitoring of the Séchillenne landslide. *Earth Surf. Dyn.* 5, 293–310. <https://doi.org/10.5194/esurf-5-293-2017>.
- Kromer, R., Walton, G., Gray, B., Lato, M., Group, R., 2019. Development and optimization of an automated fixed-location time lapse photogrammetric rock slope monitoring system. *Remote Sens.* 11 (16), 1890. <https://doi.org/10.3390/rs11161890>.
- Kuschnerus, M., Lindenbergh, R., Vos, S., 2020. Coastal change patterns from time series clustering of permanent laser scan data. *Earth Surf. Dyn. Discuss.* 1–29. <https://doi.org/10.5194/esurf-2020-34> preprint.
- Lague, D., Brodu, N., Leroux, J., 2013. Accurate 3D comparison of complex topography with terrestrial laser scanner: Application to the Rangitikei canyon (N-Z). *ISPRS J. Photogramm. Remote Sens.* 82, 10–26. <https://doi.org/10.1016/j.isprsjprs.2013.04.009>.
- Lin, Y., Zhang, L., Wang, N., 2019. A new time series change detection method for Landsat land use and land cover change. In: *10th International Workshop on the Analysis of Multitemporal Remote Sensing Images (MultiTemp)*, pp. 1–4. <https://doi.org/10.1109/Multi-Temp.2019.8866909>.
- Liu, H., Wang, L., Sherman, D., Gao, Y., Wu, Q., 2010. An object-based conceptual framework and computational method for representing and analyzing coastal morphological changes. *Int. J. Geograph. Inf. Sci.* 24 (7), 1015–1041. <https://doi.org/10.1080/13658810903270569>.
- Mayr, A., Rutzinger, M., Bremer, M., Oude Elberink, S., Stumpf, F., Geitner, C., 2017. Object-based classification of terrestrial laser scanning point clouds for landslide monitoring. *Photogram. Rec.* 32 (160), 377–397. <https://doi.org/10.1111/phor.12215>.
- Mayr, A., Rutzinger, M., Geitner, C., 2018. Multitemporal analysis of objects in 3D point clouds for landslide monitoring. *Int. Arch. Photogramm. Remote Sens. Spatial Inf. Sci.* XLII-2, 691–697. <https://doi.org/10.5194/isprs-archives-XLII-2-691-2018>.
- Miles, A., Ilic, S., Whyatt, D., James, M.R., 2019. Characterizing beach intertidal bar systems using multi-annual LiDAR data. *Earth Surf. Proc. Land.* 44 (8), 1572–1583. <https://doi.org/10.1002/esp.4594>.
- O’Dea, A., Brodie, K.L., Hartzell, P., 2019. Continuous coastal monitoring with an automated terrestrial Lidar scanner. *J. Mar. Sci. Eng.* 7 (2), 37. <https://doi.org/10.3390/jmse7020037>.
- Oppikofer, T., Jaboyedoff, M., Blikra, L., Derron, M.H., Metzger, R., 2009. Characterization and monitoring of the Aknes rockslide using terrestrial laser scanning. *Nat. Hazards Earth Syst. Sci.* 9 (3), 1003–1019. <https://doi.org/10.5194/nhess-9-1003-2009>.
- Pfeiffer, J., Zieher, T., Bremer, M., Wichmann, V., Rutzinger, M., 2018. Derivation of three-dimensional displacement vectors from multi-temporal long-range terrestrial laser scanning at the Reissenschuh Landslide (Tyrol, Austria). *Remote Sens.* 10 (11), 1688.
- Qin, R., Tian, J., Reinartz, P., 2016. 3D change detection – Approaches and applications. *ISPRS J. Photogramm. Remote Sens.* 122, 41–56. <https://doi.org/10.1016/j.isprsjprs.2016.09.013>.
- Riegl LMS, 2017. Riegl VZ-2000 (datasheet). URL: http://products.rieglusa.com/Asset/DataSheet_VZ-2000_2017-06-07.pdf (22 Dec 2020).
- Rosser, N., Lim, M., Petley, D., Dunning, S., Allison, R., 2007. Patterns of precursory rockfall prior to slope failure. *J. Geophys. Res. Earth Surf.* 112 (F4) <https://doi.org/10.1029/2006jfo00642>.
- Stumvoll, M.J., Canli, E., Engels, A., Thiebes, B., Groiss, B., Glade, T., Schweigl, J., Bertagnoli, M., 2020. The “Salcher” landslide observatory—experimental long-term monitoring in the Flysch Zone of Lower Austria. *Bull. Eng. Geol. Environ.* 79, 1831–1848. <https://doi.org/10.1007/s10064-019-01632-w>.
- Ulrich, V., Williams, J.G., Zahr, V., Anders, K., Hecht, S., Höfle, B., 2021. Measurement of rock glacier surface change over different timescales using terrestrial laser scanning point clouds. *Earth Surf. Dyn.* 9, 19–28. <https://doi.org/10.5194/esurf-9-19-2021>.
- Vos, S., Lindenbergh, R., de Vries, S., 2017. CoastScan: Continuous monitoring of coastal change using terrestrial laser scanning. *Proc. Coast. Dyn.* 2017 (233), 1518–1528.
- Walker, I.J., Davidson-Arnott, R.G.D., Bauer, B.O., Hesp, P.A., Delgado-Fernandez, I., Ollerhead, J., Smyth, T.A.G., 2017. Scale-dependent perspectives on the geomorphology and evolution of beach-dune systems. *Earth Sci. Rev.* 171, 220–253. <https://doi.org/10.1016/j.earscirev.2017.04.011>.
- Williams, J.G., Rosser, N.J., Hardy, R.J., Brain, M.J., Afana, A.A., 2018. Optimising 4-D surface change detection: an approach for capturing rockfall magnitude–frequency. *Earth Surf. Dyn.* 6, 101–119. <https://doi.org/10.5194/esurf-6-101-2018>.
- Zahr, V., Hämmerle, M., Anders, K., Hecht, S., Sailer, R., Rutzinger, M., Williams, J.G., Höfle, B., 2019. Multi-temporal 3D point cloud-based quantification and analysis of geomorphological activity at an alpine rock glacier using airborne and terrestrial LiDAR. *Permafrost Periglac. Process.* 30 (3), 222–238. <https://doi.org/10.1002/ppp.2004>.